

Prioritize Denoising Steps on Diffusion Model Preference Alignment via Explicit Denoised Distribution Estimation

Dingyuan Shi, Yong Wang[†], Hangyu Li, Xiangxiang Chu
Alibaba Group

dingyuan.shi@outlook.com, wangyong.lz@alibaba-inc.com
cyjdlhy@gmail.com, chuxiangxiang.cxx@alibaba-inc.com

Abstract

Diffusion models have shown remarkable success in text-to-image generation, making alignment methods for these models increasingly important. A key challenge is the sparsity of preference labels, which are typically available only at the terminal of denoising trajectories. This raises the issue of how to assign credit across denoising steps based on these sparse labels. In this paper, we propose Denoised Distribution Estimation (DDE), a novel method for credit assignment. Unlike previous approaches that rely on auxiliary models or hand-crafted schemes, DDE derives its strategy more explicitly. The proposed DDE directly estimates the terminal denoised distribution from the perspective of each step. It is equipped with two estimation strategies and capable of representing the entire denoising trajectory with a single model inference. Theoretically and empirically, we show that DDE prioritizes optimizing the middle part of the denoising trajectory, resulting in a novel and effective credit assignment scheme. Extensive experiments demonstrate that our approach achieves superior performance, both quantitatively and qualitatively.

1. Introduction

Diffusion models have achieved remarkable success in text-to-image generation [7, 17, 20]. A key challenge in generative modeling is alignment [12, 25], which focuses on improving a model’s ability to better align with human preferences. Alignment training has been extensively explored in the context of large language models [14, 22, 30]. Initially driven by Reinforcement Learning from Human Feedback (RLHF), alignment techniques have evolved to include approaches such as Direct Preference Optimization (DPO) [16]. The latter has gained significant attraction, inspiring a series of subsequent studies [1, 3, 29].

Despite the variety of emerging approaches, few studies have attempted to adapt Direct Preference Optimization (DPO) to text-to-image diffusion models. The primary challenge lies in the sparsity of preference labels. Specifically, human evaluators can only provide preference labels for the final *noiseless* output of generative models. In contrast, diffusion models generate images progressively, producing large numbers of *noisy* intermediate results that are difficult to label. So the question is: How can credit be assigned across the denoising steps when preference labels are only available at the terminal of the denoising trajectory?

Recent studies have explored two main approaches to address this challenge. One approach relies on auxiliary models, such as reward models [2, 6] or noisy evaluators [11]. These models essentially learn a weighting function to adaptively assign credit from the final output to each denoising step. However, this approach introduces additional training complexity, undermining the simplicity of DPO. The second approach requires no auxiliary models, maintaining the simplicity of DPO but limiting the ability to perform effective credit assignments. These methods typically rely on simple strategies, such as uniform assignment [24, 27] or discounted assignment [28] (*i.e.* placing more weight on the initial denoising steps), which may restrict the alignment potential of the model.

In this paper, we propose Denoised Distribution Estimation, a DPO method without auxiliary models for diffusion model alignment training. Instead of directly designing a hand-crafted credit assignment scheme, DDE advocates deriving the assignment mechanism via explicit estimation to the terminal denoised distribution from the perspective of each step. To this end, we propose two estimation strategies: stepwise and single-shot estimation. The stepwise estimation uses the ground-truth conditional distribution ($q(x_{t-1}|x_t, x_0)$) to estimate the model distribution ($p_\theta(x_{t-1}|x_t)$), while the single-shot estimation utilizes DDIM modeling to directly estimate the terminal distribution ($p_\theta(\hat{x}_0|x_t)$) based on an intermediate noisy latent state. By integrating these two estimation strategies, we can evaluate

[†]Corresponding Author

the entire denoising trajectory with a single model inference, which can then be leveraged during training.

We analyze our DDE both theoretically and empirically, revealing that it effectively prioritizes different denoising steps. Specifically, our estimation strategies introduce correction terms and step-specific coefficients, which lead to greater credit being assigned to the middle portion of the denoising trajectory. In other words, we naturally derive a novel credit assignment scheme by focusing solely on the estimation of the whole denoising trajectory.

We evaluate our method on both SD15 and SDXL quantitatively and qualitatively. The results demonstrate that compared with all other methods without auxiliary models, our DDE achieves state-of-the-art performance. Specifically, our DDE improves performance metrics of SD15 and SDXL by 3.3%~6.7% and 1.0%~3.1%, respectively.

Our contributions can be summarized as follows:

- We introduce DDE, a novel DPO method tailored for diffusion models without any auxiliary model. By directly estimating the terminal denoised distribution from the perspective of each step, DDE naturally derives a novel credit assignment scheme for sparse preference labels.
- We devise two estimation strategies. Theoretical and empirical analysis reveals that these strategies prioritize optimizing middle steps in denoising trajectories, which is different from existing uniform or discounted schemes.
- Experimental results show that DDE achieves state-of-the-art performance both quantitatively and qualitatively, compared to existing methods without auxiliary models.

2. Preliminaries

Diffusion Models. Traditional Denoising Diffusion Probabilistic Model (DDPM) [7] defines a forward process, which incrementally transforms a noiseless image (denoted as x_0) to pure noise (denoted as x_T) by injecting Gaussian noise as:

$$q(x_t|x_{t-1}) = \mathcal{N}(x_t; \sqrt{1 - \beta_t}x_{t-1}, \beta_t\mathbf{I}), \quad (1)$$

where β_t and $\alpha_t \equiv 1 - \beta_t$ are hyperparameters of controlling the diffusion process. The forward process can be expressed non-iteratively as:

$$q(x_t|x_0) = \mathcal{N}(x_t; \sqrt{\bar{\alpha}_t}x_0, (1 - \bar{\alpha}_t)\mathbf{I}), \quad (2)$$

where $\bar{\alpha}_t = \prod_{i=1}^t \alpha_i$ denotes the cumulative product of the scaling factor α_t .

DDPM requires a model to estimate the denoising distribution $p_\theta(x_{t-1}|x_t)$, which enables it to reverse the diffusion process and convert noise back into images. The training objective involves learning the distribution of x_{t-1} conditioned on x_0 , modeled as a Gaussian distribution:

$$q(x_{t-1}|x_t, x_0) = \mathcal{N}(x_{t-1}; \mu(x_t, x_0), \frac{1 - \bar{\alpha}_{t-1}}{1 - \bar{\alpha}_t}\beta_t\mathbf{I}), \quad (3)$$

where $\mu(x_t, x_0) = \frac{\sqrt{\bar{\alpha}_{t-1}}\beta_t}{1 - \bar{\alpha}_t}x_0 + \frac{\sqrt{\bar{\alpha}_t}(1 - \bar{\alpha}_{t-1})}{1 - \bar{\alpha}_t}x_t$. By minimizing the KL-divergence between predicted noising distribution $p_\theta(x_{t-1}|x_t)$ and the true distribution above, the diffusion model learns to denoise the randomly sampled noise x_T to x_0 progressively.

Due to the Markov property, DDPM is constrained to denoise samples incrementally, one step at a time. In contrast, Denoising Diffusion Implicit Model (DDIM) [20] incorporates a non-Markovian sub-chain, redefining the denoising process as:

$$p_\theta(\hat{x}_{t'}|x_t) = \mathcal{N}(\hat{x}_{t'}; \hat{\mu}_{\theta, t'}(x_t, t), \sigma_t\mathbf{I}), \quad (4)$$

where t' and t are two consecutive vertices within a sub-chain of the original DDPM denoising Markov chain, $\hat{\mu}_{\theta, t'}(x_t, t) = \frac{\sqrt{\bar{\alpha}_{t'}}(x_t - \sqrt{1 - \bar{\alpha}_t}\epsilon_\theta(x_t, t))}{\sqrt{\bar{\alpha}_t}} + \sqrt{1 - \bar{\alpha}_{t'} - \sigma_t^2}\epsilon_\theta(x_t, t)$ and $\sigma_t = \sqrt{\frac{1 - \bar{\alpha}_{t'}}{1 - \bar{\alpha}_t}\beta_t}$.

Direct Preference Optimization. DPO [16] aims to optimize generative models to better align with human preferences. This objective is achieved by establishing a connection between the reward model and the generative model, resulting in the following loss function:

$$\mathcal{L}_{\text{DPO}} = \mathbb{E}_{x^w, x^l \sim \mathcal{D}} \left[-\log \sigma \left(\beta \left(\log \frac{p_\theta(x^w)}{p_{ref}(x^w)} - \log \frac{p_\theta(x^l)}{p_{ref}(x^l)} \right) \right) \right] \quad (5)$$

where p_θ and p_{ref} represent the target and reference model respectively. The samples x^w and x^l constitute a paired preference set, where $x^w \succ x^l$ indicate that the win sample x^w is preferred over the lose sample x^l . The sigmoid function is denoted as σ . In this loss formulation, the differential term $(\log \frac{p_\theta(x^w)}{p_{ref}(x^w)} - \log \frac{p_\theta(x^l)}{p_{ref}(x^l)})$ serves to adjust the model to increase the probability of generating the winning sample (x^w), while decreasing that of the losing sample (x^l). The fractional components $p_{ref}(\cdot)$ keep the optimization close to the reference model, thus preventing excessive deviations.

3. Method

3.1. Overview

We introduce our Denoised Distribution Estimation (DDE) method, which adapts Direct Preference Optimization (DPO) to diffusion models. The key challenge is the sparsity of preference labels. These labels are only tagged on the terminal of denoising trajectories (*i.e.* noiseless images $x_0^w \succ x_0^l$), leaving these intermediate results ($x_t, \forall t \neq 0$) unlabeled. Previous research has addressed this issue by either utilizing auxiliary models, such as reward model [2, 6], or employing hand-crafted assignment schemes, including uniform [24, 27] and discounted strategies [28]. Our approach falls into the second category (without auxiliary models), aiming to preserve the simplicity inherent in DPO training.

Distinct from existing methods that directly target the assignment scheme design, we advocate to investigate the final impact from the perspective of each step.

To this end, the most straightforward approach would involve calculating the entire denoising trajectory. However, this would incur prohibitive training costs due to the iterative nature of the generation process. Training feasibility limits the number of model inferences that can be executed. Consequently, the final denoised distribution must be estimated with a reduced number of inferences, or preferably, in a single inference. This constraint motivates us to establish a connection between x_t and x_0 . We begin by representing $p_\theta(x_0)$ in terms of $p_\theta(x_t)$ as follows:

$$\begin{aligned} p_\theta(x_0) &= \int_{x_{1:T}} p_\theta(x_{0:T}) dx_{1:T} \\ &= \int_{x_{1:T}} q(x_T) p_\theta(x_{T-1}|x_T) \dots p_\theta(x_0|x_1) dx_{1:T} \end{aligned} \quad (6)$$

where $q(x_T)$ is a Gaussian distribution and $p_\theta(x_{t-1}|x_t)$ denotes the learned denoising distribution which constitutes the denoising trajectory.

Given a randomly sampled step t , the denoising trajectory from T to 0 can naturally be split into two segments: from T to t and from t to 0, denoted as $T \rightarrow t$ and $t \rightarrow 0$, respectively. We propose two distinct estimation strategies for each segment, as outlined below (also shown in Fig. 1).

- *Stepwise estimation for segment $T \rightarrow t$.* We estimate each step term $p_\theta(x_t|x_{t+1})$ by $q(x_t|x_{t+1}, x_0)$ (defined as Eq. 3). To further reduce the estimation error, we incorporate an importance ratio for correction.
- *Single-shot estimation for segment $t \rightarrow 0$.* We directly estimate the terminal denoised distribution of x_0 from that of x_t by using DDIM with a single model inference.

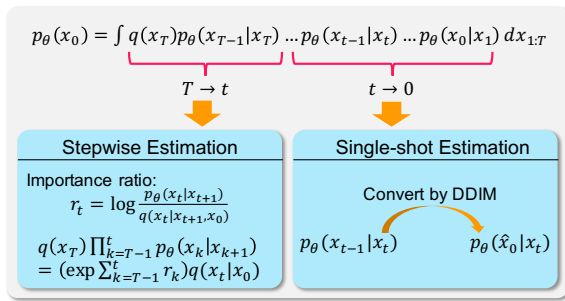


Figure 1. Our DDE adopts two estimation strategies.

Here, we present several key observations regarding our DDE method:

- *Our method explicitly builds estimation to the learned denoised distribution.* Unlike previous methods where the denoising process is modeled as a Markov sequential decision problem, our DDE explicitly estimates the learned

denoised distribution. This provides deeper insight into the denoising trajectory and a finer credit assignment scheme.

- *Both estimation strategies are indispensable.* Due to the inference pass constraints, we cannot get information about p_θ for steps prior to sampled t , making single-shot estimation inapplicable and stepwise estimation indispensable. However, both strategies can be applied after the sampled t . Our analysis indicates that the single-shot estimation significantly enhances the effectiveness of our methods, as shown in Sec. 4.5.
- *Our estimation strategies inherently prioritize the middle part of denoising trajectories.* Our estimation strategy naturally introduces a credit assignment scheme that favors the middle portion of the trajectory. In Sec. 3.4, we provide both theoretical justification and empirical evidence to prove that the prioritization significantly improves DPO optimization.

Subsequently, we introduce two estimation strategies. Table 1 summarizes key notations used throughout this paper.

Table 1. Notations

Notations	Descriptions
x_0	Noiseless sample
x_t, x_T	Noisy sample and pure noise
$\mu(x_t, x_0)$	Expectation of $q(x_{t-1} x_t, x_0)$
$p_\theta(x_{t-1} x_t)$	Estimated distribution of x_{t-1} by DDPM
$\mu_\theta(x_t, t)$	Expectation of $p_\theta(x_{t-1} x_t)$ by DDPM
$p_\theta(\hat{x}_{t'} x_t)$	Estimated distribution of $x_{t'}$ by DDIM
$\hat{\mu}_{\theta, t'}(x_t, t)$	Expectation of $p_\theta(\hat{x}_{t'} x_t)$ by DDIM

3.2. Stepwise Estimation for Segment $T \rightarrow t$

The stepwise estimation uses $q(x_t|x_{t+1}, x_0)$ (defined as Eq. 3) to estimate $p_\theta(x_t|x_{t+1})$. This approach is justifiable as the model is optimized during pretraining to minimize the KL-divergence between the above two distributions [7]. To enhance the accuracy of the estimation, we define the importance ratio as follows:

$$r_t = \log \frac{p_\theta(x_t|x_{t+1})}{q(x_t|x_{t+1}, x_0)}. \quad (7)$$

For any k within the interval $T \rightarrow t$, substituting $p_\theta(x_k|x_{k+1})$ with $\exp\{r_k\}q(x_k|x_{k+1}, x_0)$ yields

$$p_\theta(x_0) = \exp\left\{\sum_{k=t}^{T-1} r_k\right\} \int_{x_{1:t}} q(x_t|x_0) \prod_{k=t}^{T-1} p_\theta(x_{k-1}|x_k) dx_{1:t} \quad (8)$$

A comprehensive derivation is provided in Suppl. 7.1.

By adopting the stepwise estimation, the denoising segment from T to t can be simplified to a single term $q(x_t|x_0)$, with an additional correction term $\exp\{\sum_{k=t}^{T-1} r_k\}$. Term

$q(x_t|x_0)$ can be readily computed using Eq. 2. The correction term represents a summation of importance ratios, as defined in Eq. 7, where both the numerator and denominator follow the Gaussian distribution with expectation $\mu_\theta(x_{t+1}, t+1)$ and $\mu(x_{t+1}, x_0)$, respectively. By assuming both distributions have the same diagonal covariance matrix [7], fraction reduction leads to only exponential terms of the numerator and denominator and r_t can be further simplified to $-\frac{1}{2}(\|x_t - \mu_\theta(x_{t+1}, t+1)\|_2^2 - \|x_t - \mu(x_{t+1}, x_0)\|_2^2)$.

The challenge of determining r_t is primarily attributed to x_t , the noisy image sampled from $p_\theta(x_t|x_{t+1})$ during the denoising process, which remains inaccessible prior to the random sampled t . To address this, we take $\mu_\theta(x_{t+1}, t+1)$ as an estimation to x_t , as it represents the highest density of distribution $p_\theta(x_t|x_{t+1})$. Consequently, we have $r_t = \frac{1}{2}\|\mu_\theta(x_{t+1}, t+1) - \mu(x_{t+1}, x_0)\|_2^2$.

In practice, to avoid extra model inference passes when obtaining $\mu_\theta(x_{t+1}, t+1)$, we implement a delay update technique. Specifically, we record the results from the current iteration for later use. We maintain an array of length T for recording r_t and employ exponential moving average to update this value throughout the training process, which is illustrated in Algorithm 1. In line 5, the single inference pass $\mu_\theta(x_t, t)$ is employed for training in the current iteration, and it also contributes to calculating r_{t-1} for use in the subsequent iteration. Empirically, we observe that these ratios converge quickly (as shown in Fig. 7(a)), and this delay update method does not adversely affect the training process.

Algorithm 1: Delay Update of Importance Ratio

```

1 Initialize  $r[0..T-1] \leftarrow 0$ 
2 for  $training\_steps \leftarrow 1, 2, \dots$  do
3    $t \sim U[1..T]$ 
4    $x_t \leftarrow$  add noise by Eq. 2
5    $r[t-1] \leftarrow$ 
      $\alpha \cdot r[t-1] + (1-\alpha) \cdot \frac{1}{2}\|\mu_\theta(x_t, t) - \mu(x_t, x_0)\|_2^2$ 
6 end

```

Subsequently, we introduce our single-shot estimation which elaborates the term $\prod_{k=t}^1 p_\theta(x_{k-1}|x_k)$ in Eq. 8.

3.3. Single-shot Estimation for Segment $t \rightarrow 0$

Based on the Markov property of the inverse process, we have $\int_{x_{1:t-1}} \prod_{k=t}^1 p_\theta(x_{k-1}|x_k) dx_{1:t-1} = p_\theta(x_0|x_t)$. Hence, Eq. 8 can be rewritten as follows:

$$\begin{aligned}
p_\theta(x_0) &\approx \exp\left\{\sum_{k=t}^{T-1} r_k\right\} \int_{x_t} q(x_t|x_0) p_\theta(x_0|x_t) dx_t \\
&= \exp\left\{\sum_{k=t}^{T-1} r_k\right\} \mathbb{E}_{x_t \sim q(x_t|x_0)} [p_\theta(x_0|x_t)].
\end{aligned} \tag{9}$$

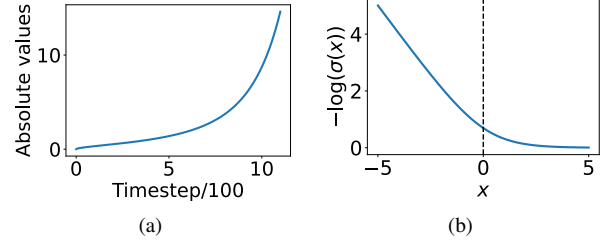


Figure 2. The left represents the value of single-shot estimation coefficients and the right denotes that of the $-\log \sigma$ function.

By viewing x_t and x_0 as consecutive vertices in a DDIM sub-chain of the original Markov chain, we have

$$p_\theta(\hat{x}_0|x_t) = \mathcal{N}(\hat{x}_0; \hat{\mu}_{\theta, t'=0}(x_t, t), \sigma_t \mathbf{I}), \tag{10}$$

where $\hat{\mu}_{\theta, t'=0}(x_t, t) = \sqrt{\bar{\alpha}_0} \left(\frac{x_t - \sqrt{1-\bar{\alpha}_t} \epsilon_\theta(x_t, t)}{\sqrt{\bar{\alpha}_t}} \right) + \sqrt{1-\bar{\alpha}_0 - \sigma_t^2} \epsilon_\theta(x_t, t)$ and $\sigma_t = \sqrt{\frac{1-\bar{\alpha}_{t-1}}{1-\bar{\alpha}_t} \beta_t}$. Therefore, the $p_\theta(x_0|x_t)$ in Eq. 9 can be calculated with only one single pass of the neural network.

Building on the above two estimation strategies, the loss can be derived as follows:

$$\begin{aligned}
\mathcal{L}_{\text{DDE}} &= \mathbb{E}_{x_0^w, x_0^l, x_t^w \sim q(x_t^w|x_0^w), x_t^l \sim q(x_t^l|x_0^l)} [-\log \sigma(\beta(\\
&\quad - \|x_0^w - \hat{\mu}_{\theta, t'=0}(x_t^w, t)\|_2^2 + \|x_0^w - \hat{\mu}_{ref, t'=0}(x_t^w, t)\|_2^2 \\
&\quad + \|x_0^l - \hat{\mu}_{\theta, t'=0}(x_t^l, t)\|_2^2 - \|x_0^l - \hat{\mu}_{ref, t'=0}(x_t^l, t)\|_2^2 \\
&\quad + \sum_{k=t}^T (r_{\theta, k}^w - r_{ref, k}^w - r_{\theta, k}^l + r_{ref, k}^l))] ,
\end{aligned} \tag{11}$$

where $\hat{\mu}_\theta$ and $\hat{\mu}_{ref}$ denote using DDIM to estimate x_0 by x_t , as introduced in Sec. 2. The detailed derivation can be found at Suppl. 7.2.

We provide an intuitive explanation for each term. For Mean Square Error (MSE) terms relating to θ , $\|x_0^w - \hat{\mu}_{\theta, t'=0}(x_t^w, t)\|_2^2$ guides the optimizer to increase the output probability of $p_\theta(x_0^w|x_t^w)$, while $\|x_0^l - \hat{\mu}_{\theta, t'=0}(x_t^l, t)\|_2^2$ decreases the model output samples like x_0^l . MSE terms with respect to the reference model penalize deviations from the reference, with large deviations pushing the optimizer toward the saturation region of the negative log-sigmoid function, thus weakening the optimization. The importance ratio terms correct these deviations, slightly modifying the MSE terms in the negative log-sigmoid function, which adjusts the optimization weight.

3.4. Prioritization Property of Our DDE Method

Our method prioritizes middle denoising steps. We find that two estimation strategies of our DDE method naturally introduce a credit assignment scheme that prioritizes the

optimization of the middle steps of denoising trajectories. Stepwise and single-shot estimation weakens the optimization of steps around 0 and T , respectively.

The stepwise estimation strategy introduces correction terms to the loss function. A larger correction term pushes the MSE terms closer into the gradient saturation region of the negative log-likelihood function, shown in Fig. 2(b), reducing the optimization effectiveness. In practice, we observe that the correction term will quickly converge, with its value diminishing for larger steps (see Sec. 4.4 for more details). This is because when the sampled t is closer to time steps around 0 (*i.e.* noiseless image), the segment $T \rightarrow t$ becomes longer, leading to higher estimation errors and larger correction terms. Consequently, this pushes the whole term into the gradient saturation region. Essentially, the stepwise estimation weakens the optimization of steps around 0.

The single-shot estimation strategy introduces weight coefficients to the predicted noise due to the DDIM modeling. These coefficients can be directly computed and increase with the rise in t , which is shown in Fig. 2(a). Larger coefficients magnify even a slight difference between the training and the reference model, pushing the term into the saturation region of the negative log-sigmoid function, as shown in Fig. 2(b). Consequently, the single-shot estimation weakens the optimization for steps near T , where the coefficients are maximal. It is critical to note that larger coefficients do not necessarily bring stronger optimization, as they influence both the training and reference model terms.

In summary, by combining both estimation strategies, our method weakens the optimization at both ends of the denoising trajectory, effectively strengthening the optimization of the middle part. We refer to this as the ‘‘prioritization property’’ of our DDE method.

Assigning credits more on the middle part is reasonable.

The prioritization property distinguishes our method from existing approaches. We initiate our comparison with the uniform credit assignment scheme [24, 27], which defines the loss function as follows:

$$\begin{aligned} \mathcal{L}_{\text{Uni}} &= \mathbb{E}_{x^w, x^l \sim \mathcal{D}} \left[\right. \\ &\quad \left. - \log \sigma \left(\beta \log \frac{p_{\theta}(x_{t-1}^w | x_t^w)}{p_{\text{ref}}(x_{t-1}^w | x_t^w)} - \beta \log \frac{p_{\theta}(x_{t-1}^l | x_t^l)}{p_{\text{ref}}(x_{t-1}^l | x_t^l)} \right) \right]. \end{aligned} \quad (12)$$

We conduct experiments based on Stable Diffusion 1.5 (SD15) [17] using Uniform loss and the performances are evaluated by CLIP model [15], which is shown in Fig. 3. The red dashed line denotes the performance of original SD15 with a score of 0.320. Training SD15 with Uniform loss for 2000 iterations yields an improvement in score to 0.331 (black dashed line). By leveraging the prioritization property inherent in our DDE method, we specifically opti-

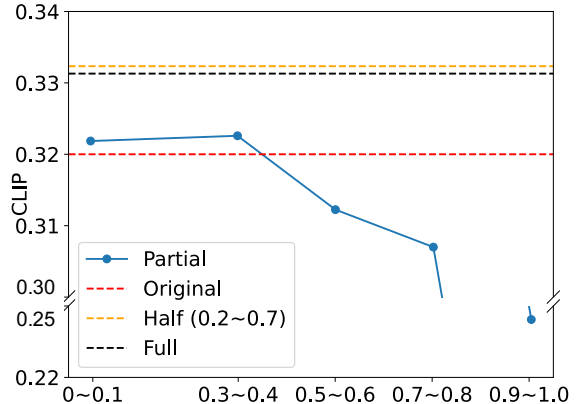


Figure 3. Comparisons among optimizing different steps. Only optimizing half of the steps can achieve a comparable performance than optimizing full steps.

mize only the intermediate subset (steps 200~700) within total 1000 denoising steps. This approach yields a further improvement to 0.332 in score. These results suggest that even a rough application of the prioritization property, by optimizing only the middle steps, demonstrates significant potential for performance improvement.

We also conduct experiments by selectively optimizing only 10% segments of the denoising steps, specifically the intervals 0~0.1, 0.3~0.4, 0.5~0.6, 0.7~0.8, and 0.9~1.0. For instance, ‘‘0~0.1’’ means optimizing the first 100 out of 1000 steps. As shown in Fig. 3, the results (denoted as blue polylines) demonstrate that optimizing just 10% of total steps can still improve performance (*i.e.* segments 0~0.1 and 0.3~0.4). However, optimizing certain segments harms the performance, particularly when focusing only on the final 10% steps, where the score drops significantly below 0.23. These findings suggest that optimization of initial denoising steps or employing a uniform optimization strategy is suboptimal.

We provide the following intuitive explanation for the above results: $x_0^w \succ x_0^l$ does not necessarily indicate that x_t^w is more preferred than x_t^l for any $t \neq 0$. More specifically, when t is large, x_t is nearly noise, the model output may not decide the image quality that affects human preference (*e.g.* aesthetic, structure, and so on). Suppressing the probability of x^l may reduce sample diversity without enhancing alignment. When t is small, the diffusion model primarily functions as a denoiser, with limited capacity to align outputs with human preferences. In this scenario, the probability of x^l may damage the denoising ability.

Besides, we also find that optimizing the first 10% steps can still improve performances. Considering that the stepwise estimation weakens the initial segment of the trajectory, this indicates that the stepwise estimation may be less important than the single-shot estimation. This finding is consistent

A panda bear as a mad scientist.

Ugly old grimy medieval man, high quality digital painting.

A cute bunny wear detailed metal armor:

A marine iguana on a surfboard.

A 8x12m room, with walls, no ceiling, ..., clear blue sky, sun not showing, one of the walls have several species of plants in vases.

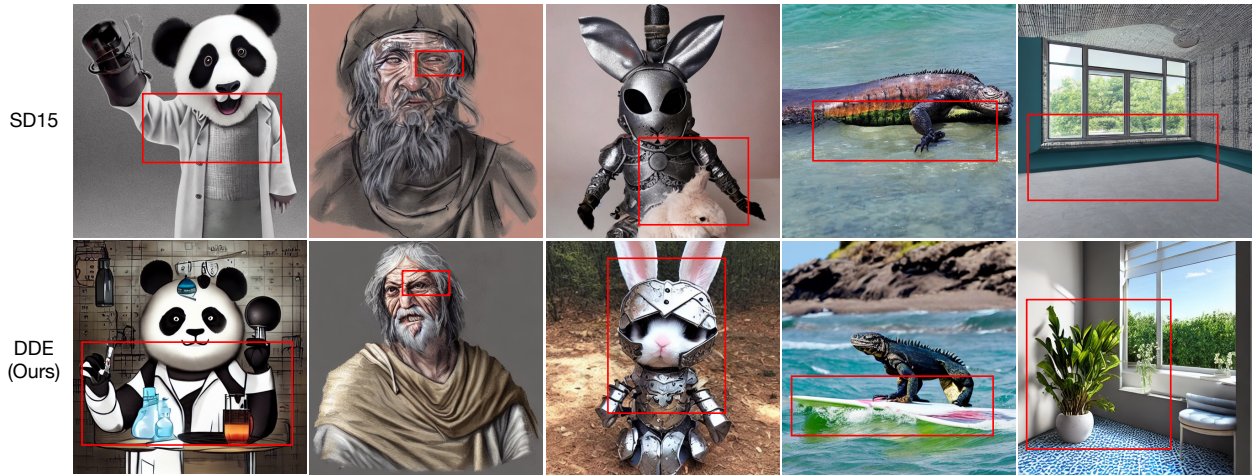


Figure 4. Our model generates images with better detail, structure, and text-alignment, compared to the SD15 model. Specifically, it can generate panda bear with tubes and flasks, which better align with “scientist” in the prompt. Additionally, the head portrait has more accurate eye detail and the rabbit is *wearing* an armor. We can generate images better containing items as prompt requested (e.g. surfboard, vases).

with results from our ablation study in Sec. 4.5.

Our experimental conclusions are summarized as follows:

- Not every step requires optimization. Optimizing half or even only 10% of steps still improves performance.
- The middle part of the trajectory may deserve more optimization. Optimizing just the middle portion yields comparable performance, consistent with the prioritization property of our DDE method.
- Optimization steps around T is less critical than those around 0. Specifically, optimizing the initial 10% steps enhances performance, while optimizing the final 10% diminishes it.

4. Experiments

4.1. Implementation Detail

We finetune the models using the Pick-a-Pic-V2 dataset¹ with the popular text-to-image models, Stable Diffusion 1.5 (SD15) and Stable Diffusion XL (SDXL). All parameters of the U-Net are trained. SD15 and SDXL are trained for 2000 and 1500 iterations, respectively. Training is conducted on 8 Nvidia H20 GPUs, each with 96GiB memory, and a batch size of 2048. Please refer to Suppl. 8.1 for more implementation details.

¹https://huggingface.co/datasets/yuvalkirstain/pickapic_v2

4.2. Quantitative Validation

To validate our approach quantitatively, we employ CLIP [15], HPS [26], and PS [9] models as annotators, each representing different types of preference. Based on these annotators, we train our methods (DDE) alongside baseline methods: Supervised Finetune (SFT), Uniform (Uni, [24, 27]), and Discounted (Disc, [28]).

Table 2. Validation of SD15

Methods	Metrics (10^{-1})		
	CLIP(↑)	HPS(↑)	PS (↑)
SD15	3.200 ± 0.657	2.622 ± 0.208	2.049 ± 0.131
SFT	3.306 ± 0.685	2.714 ± 0.245	2.101 ± 0.137
Uni	3.313 ± 0.748	2.703 ± 0.234	2.105 ± 0.134
Disc	3.317 ± 0.730	2.720 ± 0.248	2.083 ± 0.145
DDE	3.414 ± 0.627	2.725 ± 0.216	2.112 ± 0.137
DDE-Single	<u>3.386 ± 0.722</u>	<u>2.723 ± 0.204</u>	2.117 ± 0.129
DDE-Step	3.168 ± 0.671	2.600 ± 0.671	2.056 ± 0.123

We conducted an extensive comparison on both SD15 and SDXL, illustrated in the upper sections of Table 2 and Table 3, respectively. Our proposed approach not only enhances the performance of the base models but also surpasses all other baselines. Specifically, our DDE improves SD15 by 6.7%, 3.9%, and 3.3% in terms of CLIP, HPS and PS, respectively. Furthermore, it improves SDXL by 1.4%, 1.0%, and 3.1% across the same metrics.

In addition to comparing the mean value of all validation images, we also analyze the beat ratios. As shown

Table 3. Validation of SDXL

Methods	Metrics (10^{-1})		
	CLIP (\uparrow)	HPS (\uparrow)	PS (\uparrow)
SDXL	3.664 ± 0.579	2.803 ± 0.172	2.154 ± 0.145
Uni	3.699 ± 0.542	2.806 ± 0.168	2.191 ± 0.134
Disc	3.677 ± 0.540	2.742 ± 0.155	2.136 ± 0.130
DDE	3.715 ± 0.521	2.831 ± 0.175	2.224 ± 0.137

in Fig. 5), our DDE outperforms SD15 with beat ratios of 65.6%, 76.7%, 72.7% in terms of CLIP, HPS, and PS, respectively, surpassing other baseline methods. Further quantitative comparisons are provided in Suppl. 8.2.

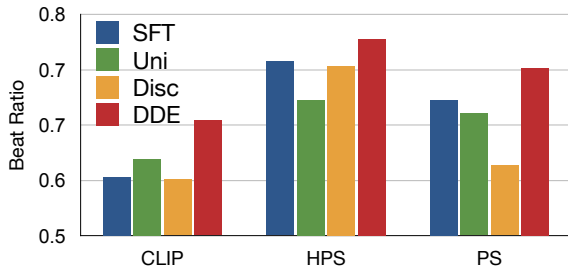


Figure 5. Beat ratio comparison. Our DDE method achieves the highest beat ratios across all validation metrics than other baselines.

4.3. Qualitative Validation

In this section, we conduct a qualitative comparison between our model and the baseline models and provide some illustrative examples. More generated cases are also available in Suppl. 8.3.

As shown in Fig. 4, our model surpasses SD15 in generating images with superior details, structure, and text alignment. For instance, the “panda scientist” produced by using our approach holds on flasks and tubes, exhibiting enhanced detail generation capability compared to the base models. The head portrait generated by the base model suffers eye structure collapse, which our model successfully avoids. Furthermore, our model produces rabbit *wearing* an armor that is more aligned with the given prompt. Additionally, the generated image has a better view of the surfboard as the prompt request, and the room corner we produce displays more details and a clearer view.

Our model also enhances the SDXL model, as illustrated in Fig. 6. For the city view generation, we maintain the detail of windows on the buildings more effectively than the base model. Our approach accurately generates a human hand with the right number of fingers, and a dancer with the correct body structure. The text generated by our model is clearer, aligning precisely with the prompt. Moreover, the inverted reflections in water generated by our model exhibit more accurate structural details.

4.4. How the Correction Terms Prioritize Steps

We now explain that our correction terms brought by our stepwise estimation strategy weaken optimizing those steps around 0. It can be shown in Fig. 7(a) that the correction terms quickly converge as training iteration reaches 100. The distribution of values is illustrated in Fig. 7(b), clearly indicating a decrease in values as the number of steps increases. Notably, a larger correction term pushes the value into the saturation domain of the negative log-sigmoid function, thus weakening the optimization. Therefore, our correction terms weaken the optimization of steps around 0.

4.5. Ablation study

We conduct experiments using only one of the two estimation strategies described above. Specifically, “DDE-Step” denotes only adopting the stepwise estimation, while “DDE-Single” refers to using the single-shot estimation alone. The results are shown in the bottom section of Table 2.

When applying only the single-shot estimation, all metrics exhibit performance at or above the level of DDE, demonstrating the effectiveness of this strategy. In contrast, when only the stepwise estimation is used, all metrics show a decrease in performance, even falling below the baseline model. This observation is consistent with the analysis in Sec. 3.4. It is important to note that the stepwise estimation weakens optimization at the initial stage while strengthening it at the steps around T . Consequently, optimizing only the first or last 10% of steps either improves or harms performance, respectively. Therefore, using the stepwise estimation alone weakens the critical steps essential for optimal performance, leading to suboptimal outcomes.

However, this does not mean the stepwise strategy is ineffective. In fact, when both strategies are combined, performance enhancements are observed in 2 out of 3 metrics. This improvement arises from the single-shot estimation, which strengthens optimization at the initial steps, thereby mitigating the negative impact of the stepwise estimation and ultimately resulting in superior outcomes.

5. Related work

Reinforcement Learning from Human Feedback (RLHF).

Using human feedback as a supervision signal in Reinforcement Learning (RL) has been proposed [10] and evolved to a preference-based paradigm for better robustness [4, 8, 13].

RLHF has been recently utilized in generative models, particularly large language models [14, 22, 30]. A typical RLHF framework trains a reward model using preference data, and then applies a proximal policy optimization (PPO) algorithm [19] to optimize the policy (*i.e.*, the generative model). One key drawback of this approach is the high computational cost. To address this issue, Direct Preference Optimization (DPO) was proposed [16] based on the con-

A city view of above, manga style. *A DJ mixing in a futuristic cyberpunk nightclub, 8k UHD, RAW photo.* *Dancing on water.* *Giant orange glowing humanoid with a sign saying "im real"...* *A flat roof villa near a river with black wall and huge windows, between river and house, there is a bank.*

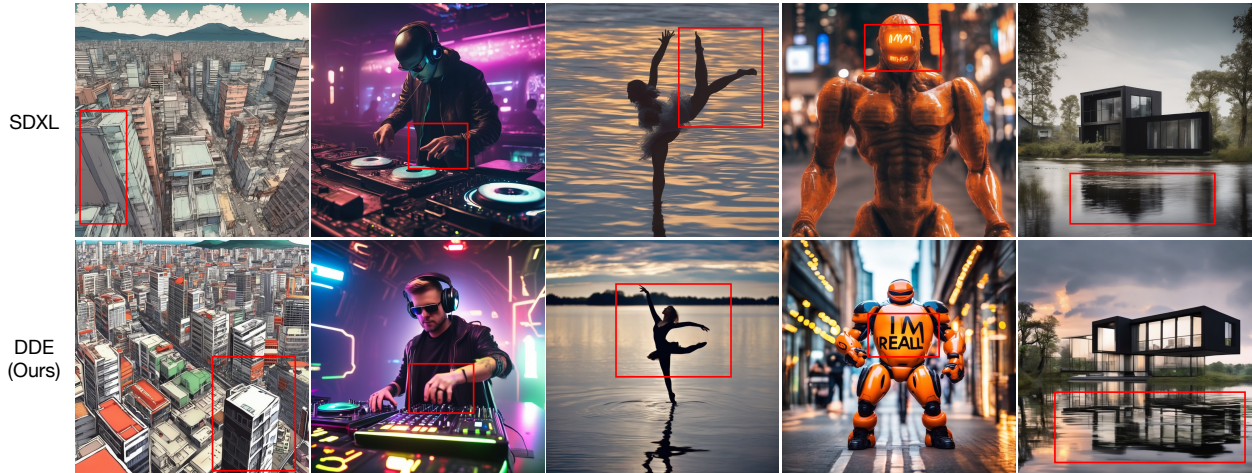


Figure 6. Our model generates images with better detail, structure, text-alignment than SDXL model. We can generate building retaining window details and human hand with right number of fingers. The dancing body structure can be kept and the requested text as well as the reflection in the water can be correctly generated.

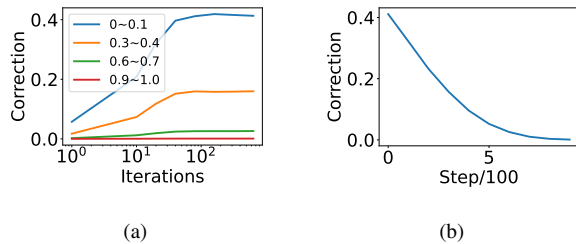


Figure 7. The importance ratios converge within 100 training iterations (left). The value of correction terms become larger when t is closer to 0 (right).

nection between the optimal policy and the reward model. This approach has gained significant attention and has been explored in various studies [1, 3, 29]. However, extending DPO to diffusion models remains an underexplored area.

Alignment training for diffusion model. Diffusion models establish a connection between a sample distribution (*e.g.* a Gaussian distribution) and the data distribution [7]. By learning the inverse process (score matching [21]), these models can generate images from randomly sampled noise. Techniques like latent space conversion [17] and DDIM sampling [20] further enhance both the efficiency and effectiveness of the generation process. Recent studies have explored applying the Direct Preference Optimization (DPO) algorithm to align diffusion models [2, 6, 11, 24, 27, 28]. One of the main challenges in applying DPO to diffusion models is the sparsity of preference labels. The credit assignment strategy

in these methods forms two major streams of thought.

The first stream relies on auxiliary models. Some approaches, like those in [2, 6], train a reward model and apply reinforcement learning for optimization. Others, such as [11], train an evaluator for noisy latents, similar to classifier-guided methods [5] that use classifiers on noisy images. While effective, these methods introduce training complexity, which detracts from the simplicity of DPO.

The second stream avoids auxiliary models, but this makes credit assignment across denoising steps more challenging. For example, [24, 27] proposes a rough approximation to uniformly optimize all steps, while [28] introduces discounted factors, handcrafting a weighting function that prioritizes early denoising steps. However, these methods rely on heuristics and fail to estimate the impact of each step with sufficient accuracy.

Our method falls into the second stream which is free from the complexity of auxiliary models. Also, it attempts to avoid the roughly hand-crafted credit assignment scheme and derives a novel scheme by revealing the impact on the terminal denoised distribution of each step.

6. Conclusion

In this paper, we introduce Denoised Distribution Estimation (DDE), a novel direct preference optimization method tailored for diffusion models. Our DDE addresses the challenge of credit assignment across denoising steps, an issue stemming from the sparsity of preference labels, by leveraging an enhanced insight into the denoising process. DDE

incorporates two estimation strategies that evaluate the impact of each denoising step on the final outcome. Our analysis reveals that these two strategies implicitly prioritize the optimization of intermediate steps within the denoising trajectory, which is a key distinction from existing methods. Experimental evaluations show that our approach outperforms previous methods. It generates images with superior metrics of CLIP, HPS, and PS and achieves better alignment of human preference in terms of detail, text-image coherence, and structures.

References

- [1] Mohammad Gheshlaghi Azar, Zhaohan Daniel Guo, Bilal Piot, Rémi Munos, Mark Rowland, Michal Valko, and Daniele Calandriello. A general theoretical paradigm to understand learning from human preferences. In *International Conference on Artificial Intelligence and Statistics, 2-4 May 2024, Palau de Congressos, Valencia, Spain*, pages 4447–4455. PMLR, 2024. 1, 8
- [2] Kevin Black, Michael Janner, Yilun Du, Ilya Kostrikov, and Sergey Levine. Training diffusion models with reinforcement learning. In *The Twelfth International Conference on Learning Representations, ICLR 2024, Vienna, Austria, May 7-11, 2024*. OpenReview.net, 2024. 1, 2, 8
- [3] Zixiang Chen, Yihe Deng, Huizhuo Yuan, Kaixuan Ji, and Quanquan Gu. Self-play fine-tuning converts weak language models to strong language models. In *Forty-first International Conference on Machine Learning, ICML 2024, Vienna, Austria, July 21-27, 2024*. OpenReview.net, 2024. 1, 8
- [4] Paul F. Christiano, Jan Leike, Tom B. Brown, Miljan Martic, Shane Legg, and Dario Amodei. Deep reinforcement learning from human preferences. In *Advances in Neural Information Processing Systems 30: Annual Conference on Neural Information Processing Systems 2017, December 4-9, 2017, Long Beach, CA, USA*, pages 4299–4307, 2017. 7
- [5] Prafulla Dhariwal and Alexander Quinn Nichol. Diffusion models beat gans on image synthesis. In *Advances in Neural Information Processing Systems 34: Annual Conference on Neural Information Processing Systems 2021, NeurIPS 2021, December 6-14, 2021, virtual*, pages 8780–8794, 2021. 8
- [6] Ying Fan, Olivia Watkins, Yuqing Du, Hao Liu, Moonkyung Ryu, Craig Boutilier, Pieter Abbeel, Mohammad Ghavamzadeh, Kangwook Lee, and Kimin Lee. DPOK: reinforcement learning for fine-tuning text-to-image diffusion models. *CoRR*, abs/2305.16381, 2023. 1, 2, 8
- [7] Jonathan Ho, Ajay Jain, and Pieter Abbeel. Denoising diffusion probabilistic models. In *Advances in Neural Information Processing Systems 33: Annual Conference on Neural Information Processing Systems 2020, NeurIPS 2020, December 6-12, 2020, virtual*, 2020. 1, 2, 3, 4, 8
- [8] Borja Ibarz, Jan Leike, Tobias Pohlen, Geoffrey Irving, Shane Legg, and Dario Amodei. Reward learning from human preferences and demonstrations in atari. In *Advances in Neural Information Processing Systems 31: Annual Conference on Neural Information Processing Systems 2018, NeurIPS 2018, December 3-8, 2018, Montréal, Canada*, pages 8022–8034, 2018. 7
- [9] Yuval Kirstain, Adam Polyak, Uriel Singer, Shahbuland Matiana, Joe Penna, and Omer Levy. Pick-a-pic: An open dataset of user preferences for text-to-image generation. In *Advances in Neural Information Processing Systems 36: Annual Conference on Neural Information Processing Systems 2023, NeurIPS 2023, New Orleans, LA, USA, December 10-16, 2023*, 2023. 6
- [10] W. Bradley Knox and Peter Stone. Interactively shaping agents via human reinforcement: the TAMER framework. In *Proceedings of the 5th International Conference on Knowledge Capture (K-CAP 2009), September 1-4, 2009, Redondo Beach, California, USA*, pages 9–16. ACM, 2009. 7
- [11] Zhanhao Liang, Yuhui Yuan, Shuyang Gu, Bohan Chen, Tiankai Hang, Ji Li, and Liang Zheng. Step-aware preference optimization: Aligning preference with denoising performance at each step. *CoRR*, abs/2406.04314, 2024. 1, 8
- [12] Buhua Liu, Shitong Shao, Bao Li, Lichen Bai, Zhiqiang Xu, Haoyi Xiong, James Kwok, Sumi Helal, and Zeke Xie. Alignment of diffusion models: Fundamentals, challenges, and future. *CoRR*, abs/2409.07253, 2024. 1
- [13] James MacGlashan, Mark K. Ho, Robert Tyler Loftin, Bei Peng, Guan Wang, David L. Roberts, Matthew E. Taylor, and Michael L. Littman. Interactive learning from policy-dependent human feedback. In *Proceedings of the 34th International Conference on Machine Learning, ICML 2017, Sydney, NSW, Australia, 6-11 August 2017*, pages 2285–2294. PMLR, 2017. 7
- [14] Long Ouyang, Jeffrey Wu, Xu Jiang, Diogo Almeida, Carroll L. Wainwright, Pamela Mishkin, Chong Zhang, Sandhini Agarwal, Katarina Slama, Alex Ray, John Schulman, Jacob Hilton, Fraser Kelton, Luke Miller, Maddie Simens, Amanda Askell, Peter Welinder, Paul F. Christiano, Jan Leike, and Ryan Lowe. Training language models to follow instructions with human feedback. In *Advances in Neural Information Processing Systems 35: Annual Conference on Neural Information Processing Systems 2022, NeurIPS 2022, New Orleans, LA, USA, November 28 - December 9, 2022*. 1, 7
- [15] Alec Radford, Jong Wook Kim, Chris Hallacy, Aditya Ramesh, Gabriel Goh, Sandhini Agarwal, Girish Sastry, Amanda Askell, Pamela Mishkin, Jack Clark, Gretchen Krueger, and Ilya Sutskever. Learning transferable visual models from natural language supervision. In *Proceedings of the 38th International Conference on Machine Learning, ICML 2021, 18-24 July 2021, Virtual Event*, pages 8748–8763. PMLR, 2021. 5, 6
- [16] Rafael Rafailov, Archit Sharma, Eric Mitchell, Christopher D. Manning, Stefano Ermon, and Chelsea Finn. Direct preference optimization: Your language model is secretly a reward model. In *Advances in Neural Information Processing Systems 36: Annual Conference on Neural Information Processing Systems 2023, NeurIPS 2023, New Orleans, LA, USA, December 10 - 16, 2023*, 2023. 1, 2, 7
- [17] Robin Rombach, Andreas Blattmann, Dominik Lorenz, Patrick Esser, and Björn Ommer. High-resolution image

- synthesis with latent diffusion models. In *IEEE/CVF Conference on Computer Vision and Pattern Recognition, CVPR 2022, New Orleans, LA, USA, June 18-24, 2022*, pages 10674–10685. IEEE, 2022. 1, 5, 8
- [18] Tim Salimans, Ian J. Goodfellow, Wojciech Zaremba, Vicki Cheung, Alec Radford, and Xi Chen. Improved techniques for training gans. In *Advances in Neural Information Processing Systems 29: Annual Conference on Neural Information Processing Systems 2016, December 5-10, 2016, Barcelona, Spain*, pages 2226–2234, 2016. 3
- [19] John Schulman, Filip Wolski, Prafulla Dhariwal, Alec Radford, and Oleg Klimov. Proximal policy optimization algorithms. *CoRR*, abs/1707.06347, 2017. 7
- [20] Jiaming Song, Chenlin Meng, and Stefano Ermon. Denoising diffusion implicit models. In *9th International Conference on Learning Representations, ICLR 2021, Virtual Event, Austria, May 3-7, 2021*. OpenReview.net, 2021. 1, 2, 8
- [21] Yang Song, Jascha Sohl-Dickstein, Diederik P. Kingma, Abhishek Kumar, Stefano Ermon, and Ben Poole. Score-based generative modeling through stochastic differential equations. In *9th International Conference on Learning Representations, ICLR 2021, Virtual Event, Austria, May 3-7, 2021*. OpenReview.net, 2021. 8
- [22] Nisan Stiennon, Long Ouyang, Jeff Wu, Daniel M. Ziegler, Ryan Lowe, Chelsea Voss, Alec Radford, Dario Amodei, and Paul F. Christiano. Learning to summarize from human feedback. *CoRR*, abs/2009.01325, 2020. 1, 7
- [23] Christian Szegedy, Vincent Vanhoucke, Sergey Ioffe, Jonathon Shlens, and Zbigniew Wojna. Rethinking the inception architecture for computer vision. In *2016 IEEE Conference on Computer Vision and Pattern Recognition, CVPR 2016, Las Vegas, NV, USA, June 27-30, 2016*, pages 2818–2826. IEEE Computer Society, 2016. 3
- [24] Bram Wallace, Meihua Dang, Rafael Rafailov, Linqi Zhou, Aaron Lou, Senthil Purushwalkam, Stefano Ermon, Caiming Xiong, Shafiq Joty, and Nikhil Naik. Diffusion model alignment using direct preference optimization. In *IEEE/CVF Conference on Computer Vision and Pattern Recognition, CVPR 2024, Seattle, WA, USA, June 16-22, 2024*, pages 8228–8238. IEEE, 2024. 1, 2, 5, 6, 8
- [25] Yufei Wang, Wanjuan Zhong, Liangyou Li, Fei Mi, Xingshan Zeng, Wenyong Huang, Lifeng Shang, Xin Jiang, and Qun Liu. Aligning large language models with human: A survey. *CoRR*, abs/2307.12966, 2023. 1
- [26] Xiaoshi Wu, Yiming Hao, Keqiang Sun, Yixiong Chen, Feng Zhu, Rui Zhao, and Hongsheng Li. Human preference score v2: A solid benchmark for evaluating human preferences of text-to-image synthesis. *CoRR*, abs/2306.09341, 2023. 6
- [27] Kai Yang, Jian Tao, Jiafei Lyu, Chunjiang Ge, Jiabin Chen, Weihao Shen, Xiaolong Zhu, and Xiu Li. Using human feedback to fine-tune diffusion models without any reward model. In *IEEE/CVF Conference on Computer Vision and Pattern Recognition, CVPR 2024, Seattle, WA, USA, June 16-22, 2024*, pages 8941–8951. IEEE, 2024. 1, 2, 5, 6, 8
- [28] Shentao Yang, Tianqi Chen, and Mingyuan Zhou. A dense reward view on aligning text-to-image diffusion with preference. In *Forty-first International Conference on Machine Learning, ICML 2024, Vienna, Austria, July 21-27, 2024*. OpenReview.net, 2024. 1, 2, 6, 8
- [29] Zheng Yuan, Hongyi Yuan, Chuanqi Tan, Wei Wang, Songfang Huang, and Fei Huang. RRHF: rank responses to align language models with human feedback without tears. *CoRR*, abs/2304.05302, 2023. 1, 8
- [30] Daniel M. Ziegler, Nisan Stiennon, Jeffrey Wu, Tom B. Brown, Alec Radford, Dario Amodei, Paul F. Christiano, and Geoffrey Irving. Fine-tuning language models from human preferences. *CoRR*, abs/1909.08593, 2019. 1, 7

Prioritize Denoising Steps on Diffusion Model Preference Alignment via Explicit Denoised Distribution Estimation

Supplementary Material

7. Derivation

7.1. Derivation of the Loss Function Defined in Eq. 8

By substituting $p_\theta(x_t|x_{t+1})$ with $e^{r_t}q(x_t|x_{t+1}, x_0)$ in Eq. 6, we obtain:

$$\begin{aligned}
 p_\theta(x_0) &= \int_{x_{1:T}} q(x_T)p_\theta(x_{T-1}|x_T)\dots p_\theta(x_0|x_1)dx_{1:T} \\
 &= \exp\left\{\sum_{k=t}^{T-1} r_k\right\} \int_{x_{1:T}} q(x_T) \prod_{k=T-1}^t q(x_k|x_{k+1}, x_0) \\
 &\quad \prod_{k=t}^1 p_\theta(x_{k-1}|x_k)dx_{1:T}
 \end{aligned}
 \tag{13}$$

We now consider the term $q(x_T) \prod_{k=T-1}^t q(x_k|x_{k+1}, x_0)$. Noting that $q(x_T)$ is independent of x_0 , we have $q(x_T) = q(x_T|x_0)$. Applying Bayes' theorem, it follows that:

$$\begin{aligned}
 &\int q(x_T|x_0)q(x_{T-1}|x_T, x_0)\dots dx_{t:T-1}dx_T \\
 &= \int q(x_T, x_{T-1}|x_0)dx_T\dots dx_{t:T-1} \\
 &= \int q(x_{T-1}|x_0)q(x_{T-2}|x_{T-1}, x_0)\dots dx_{t:T-2}dx_{T-1} \\
 &= \int q(x_{T-2}|x_0)\dots dx_{t:T-2} \\
 &= \int q(x_t|x_0)dx_t
 \end{aligned}
 \tag{14}$$

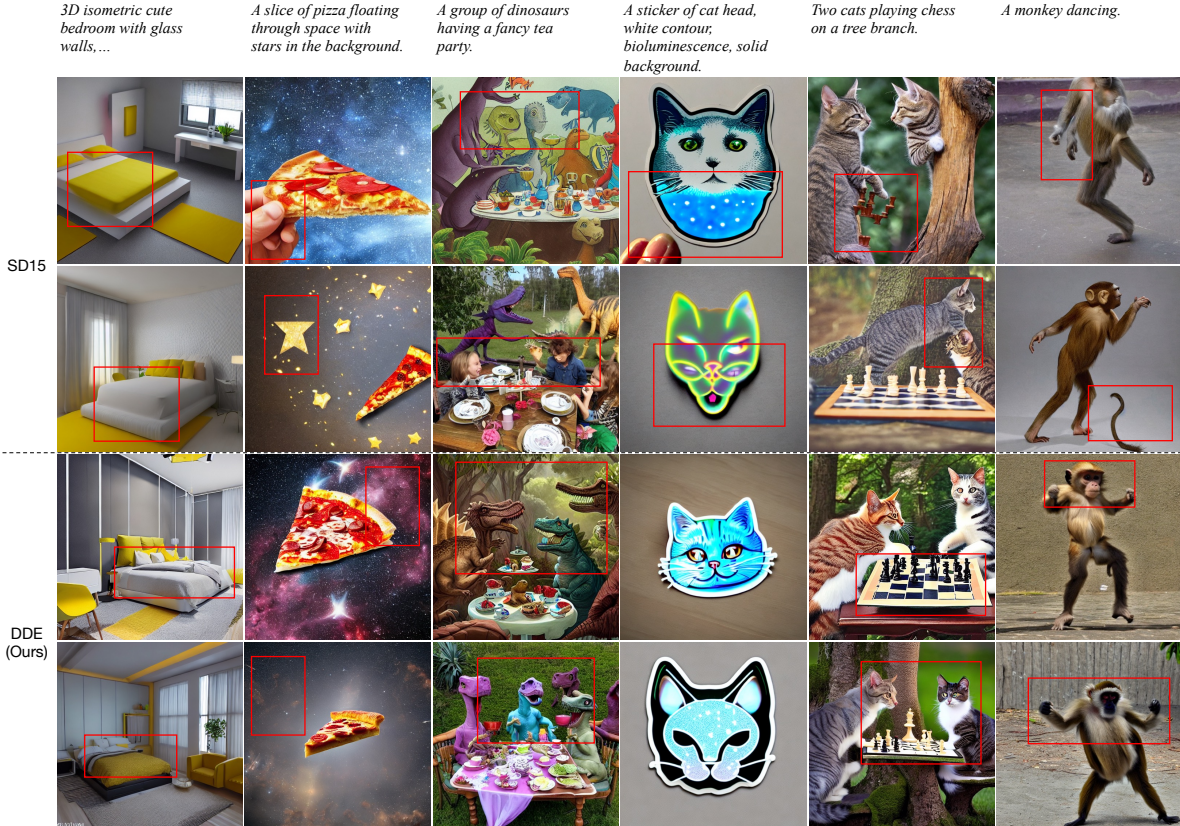


Figure 8. Extended comparative analysis between our DDE and SD15 model. Our model demonstrates superiority in generating images with enhanced details (e.g. beds covered with pillows and quilts, dinosaurs' heads with finer texture), producing more coherent layouts (e.g. pizza floating without human hand and cats playing chess at proper position), and avoiding structural collapse (e.g. cat-like stickers and the dancing monkey's structure can be retained).

Thus, we obtain:

$$p_\theta(x_0) \approx \exp\left\{\sum_{k=t}^{T-1} r_k\right\} \int_{x_{1:t}} q(x_t|x_0) \prod_{k=t}^1 p_\theta(x_{k-1}|x_k) dx_{1:t} \quad (15)$$

7.2. Derivation of Eq. 11

By replacing $p_\theta(x_0)$ and $p_{ref}(x_0)$ in the logarithmic term of Eq. 5 with Eq. 9, we obtain:

$$\begin{aligned} & \log \frac{p_\theta(x_0^w)}{p_{ref}(x_0^w)} \\ &= \sum_{k=t}^T (r_{\theta,k}^w - r_{ref,k}^w) + \log \frac{\mathbb{E}_{x_t^w \sim q(x_t^w|x_0)} [p_\theta(x_0^w|x_t)]}{\mathbb{E}_{x_t^w \sim q(x_t^w|x_0)} [p_{ref}(x_0^w|x_t)]} \end{aligned} \quad (16)$$

To avoid the high computation cost of the integral calculation related to the expectation, we employ the Monte Carlo method, using a single point $x_t \sim q(x_t|x_0)$ for estimation. Applying this estimation as model input to both the target

and reference models, we derive:

$$\begin{aligned} & \log \frac{\mathbb{E}_{x_t^w \sim q(x_t^w|x_0)} [p_\theta(x_0^w|x_t)]}{\mathbb{E}_{x_t^w \sim q(x_t^w|x_0)} [p_{ref}(x_0^w|x_t)]} \\ &= -\|x_0^w - \hat{\mu}_{\theta,t'=0}(x_t^w, t)\|_2^2 + \|x_0^w - \hat{\mu}_{ref,t'=0}(x_t^w, t)\|_2^2 \end{aligned} \quad (17)$$

The derivations of the terms $\frac{p_\theta(x_0^w)}{p_{ref}(x_0^w)}$ and $\frac{p_\theta(x_0^l)}{p_{ref}(x_0^l)}$ follow the same procedure. Consequently, the total loss function is given by:

$$\begin{aligned} & \mathcal{L}_{DDE} \\ &= \mathbb{E}_{x_0^w, x_0^l, x_t^w \sim q(x_t^w|x_0^w), x_t^l \sim q(x_t^l|x_0^l)} [-\log \sigma(\beta(\\ & - \|x_0^w - \hat{\mu}_{\theta,t'=0}(x_t^w, t)\|_2^2 + \|x_0^w - \hat{\mu}_{ref,t'=0}(x_t^w, t)\|_2^2 \\ & + \|x_0^l - \hat{\mu}_{\theta,t'=0}(x_t^l, t)\|_2^2 - \|x_0^l - \hat{\mu}_{ref,t'=0}(x_t^l, t)\|_2^2 \\ & + \sum_{k=t}^T (r_{\theta,k}^w - r_{ref,k}^w - r_{\theta,k}^l + r_{ref,k}^l))] \end{aligned} \quad (18)$$

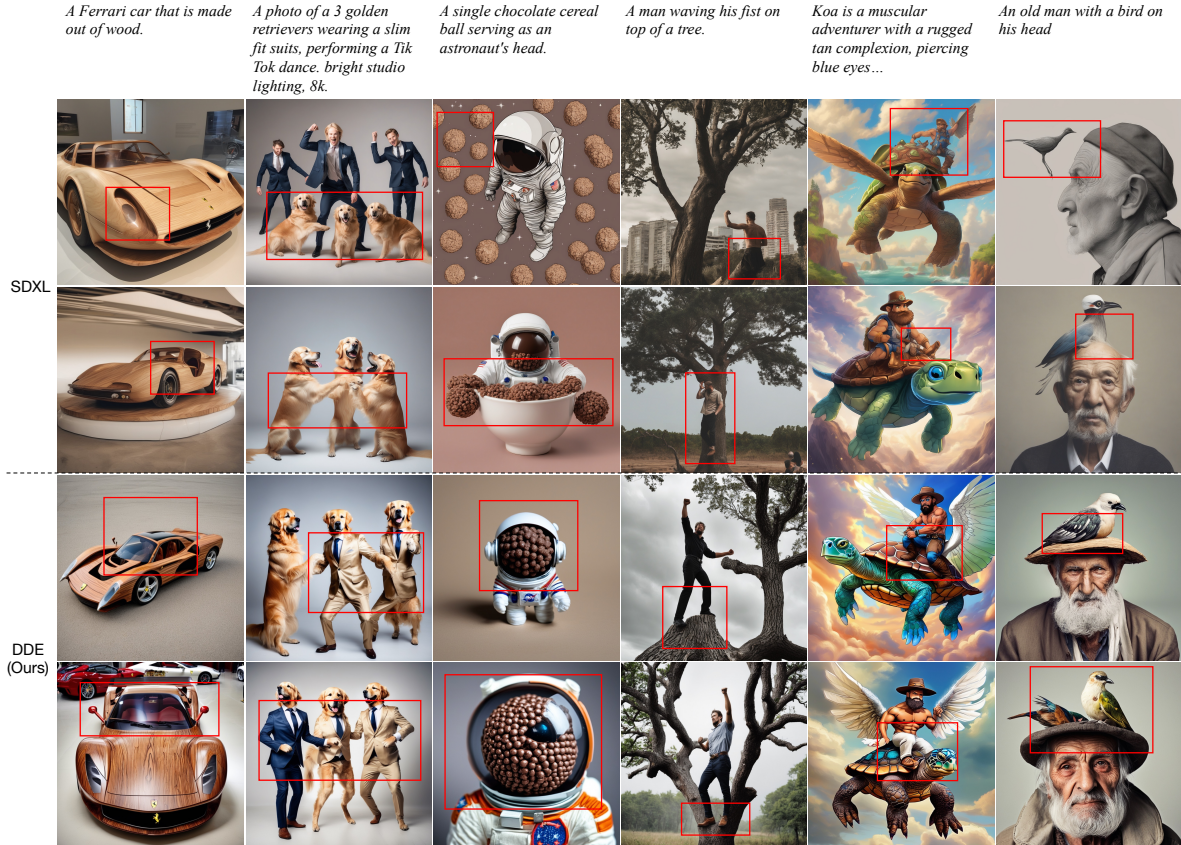


Figure 9. Extended comparative analysis between our DDE and SDXL model. The results indicate our DDE excels in producing more intricately detailed car models. Additionally, DDE exhibits a heightened ability to follow prompt instructions (e.g. the dogs wearing slim suits, the astronaut’s head shaping like a cereal ball, and the man waving fists on a tree). Furthermore, our model consistently maintains accurate structural integrity in interfaces, such as those between cartoon figure and the turtle, as well as between birds and human heads.

8. Extended Experiments

8.1. Implementation Details

We employ a constant learning rate with a warm-up schedule, finalizing at 2.05×10^{-5} . The hyper-parameters β and μ are set to 5000 and 0.1 respectively. To optimize computational efficiency, both gradient accumulation and gradient checkpointing techniques are utilized. The validation set of Pick-a-pic dataset contains over 300 prompts. For each prompt, we generate eight images and subsequently evaluate the scores using various models.

Our source code is available at <https://anonymous.4open.science/r/DDE-B6C8/README.md>.

8.2. More Quantitative Evaluation

We conduct a quantitative evaluation of the Inception Score (IS) [18] for both SD15 and SDXL models. Each model is executed with generating 50 images for each class in the ImageNet dataset, resulting in a total of 50,000 images. The prompt used for generation is formatted as “A photo of <class name>”. To address ambiguity, we specify “bird crane” and “machine crane” for class “crane”. For the duplicated class “maillot”, we distinguish between “maillot swimsuit” and “maillot tanksuit”. These minor modifications do not significantly impact the results. The Inception Scores are calculated using the Inception-V3 model [23]. A comparative analysis of the scores is presented in Table 4, indicating that our alignment training enhances the Inception Score.

It is important to note that these models are not trained on ImageNet. Therefore, we consider this comparison as a weak validation, which is included in the supplementary material.

	SD15	SDXL
Before Training	120.6 ± 2.4	173.9 ± 3.6
After Training	122.9 ± 2.4	190.1 ± 2.2

Table 4. Inception Score

8.3. Extended Qualitative Evaluation

In this subsection, we present additional generated case comparisons to substantiate the superior quality of our method.

A comparison of the SD15 model can be found in Fig. 8. Our model demonstrates superior proficiency in generating intricate content. For instance, the beds produced by our model display quilts and pillows with finer folds. Moreover, the images generated by our method exhibit increased coherence, as the pizza appears to float without the presence of human hands and the background stars exhibit a more natural look. The dinosaurs’ heads our model generate

possess finer structures and textures compared to the base model. The cat stickers generated by our DDE maintain the structural integrity of the cat head. Additionally, our model excels in generating images with a more appropriate layout, as evidenced by the two cats playing chess with a clearer chessboard and more natural positions than those generated by the base model. The dancing monkeys created by our method better preserve body structures than those produced by the base model.

The comparative analysis of the SDXL model is depicted in Fig. 9. For cars made out of woods, our model exhibits superior detail generation. It also demonstrates enhanced comprehension of prompts, accurately depicting dogs *wearing* suits, and astronauts with heads composed of cereal balls, as specified. Our generated human figures exhibit postures and positions that better adhere to the prompt requirements compared to those produced by the SDXL model. Additionally, our model effectively generates cartoon figures, avoiding structure collapse and providing a clearer interface between the man’s head and the bird.